Numerical Investigation on Cracking Behavior of Shield Tunnel Lining Subjected to Surface Loading: A Parametric Study

Jiachong Xie, Jinchang Wang(✉), Weiming Huang, Zhongxuan Yang, and Rongqiao Xu

Department of Civil Engineering, Zhejiang University, Hangzhou 310058, China
wjc501@zju.edu.cn

Abstract. An optimized finite element method (FEM) based on layer structure method has been put forward, which combined the nonlinear behavior of both the structure and the soil surrounding. The lining is simulated with solid element and meshed finely, while the longitudinal joint between segments is modeled by 6-node line interface element. Nonlinear mechanical behaviors of soil, concrete, reinforcement and interfaces are considered with advanced material models. A parameter study is conducted to reveal the influence of several concerning parameters such as the rotation angle of the ring, the width of surface loading, the offset of surface loading and the depth of the tunnel. To better illustrate the result, several indexes including maximum crack width, crack index and crack ratio is introduced to evaluate and forecast crack behavior. The results show that the crack-resistant ability of the tunnel is slightly enhanced as the rotation angle of the ring increases. A more unfavorable influence can be brought to linings by the shift of the surface loading when its offsetting is smaller than 30 m in the case. However, the influence on segment cracking caused by the change of the tunnel depth is complicated when stress redistribution after tunnel excavation is considered, and there is an unfavorable buried depth when the crack ratio reaches maximum. Finally, a simple fitting equation, which is based on the previously mentioned numerical simulation, is provided to establish the relationship between the horizontal ovalisation and the crack ratio.

1 Introduction

Linked by bolts and rubber packers, shield tunnel segments are assembled into a massive structure with a certain degree of flexibility, while it has quite a strong resistance of oval-shaping and cracking. Even if owning excellent working performance, the shield tunnel and its segments still suffer from overrunning ovalisation and other diseases because of intense environmental disturbances such as adjacent excavation, surface loading and tunnel under-crossing during operation. Among them, unexpected surface loading in the proximity of tunnel may be the most common one. It is generally accepted that the tunnel structure in soft soil areas is more sensitive to the surface loading. Besides of the ovalisation and settlement of the tunnel, diseases like concrete cracking, water leakage and segment misalignment appear frequently within the affected subway section

Y. Liu et al. (Eds.): GeoChina 2021, SUCI, pp. 65–79, 2021.
https://doi.org/10.1007/978-3-030-80316-2_7

(Shao et al. 2016). Thus, it is of great significance for practical engineering to analyze the deformation features and cracking characteristics of concrete segments under the condition of surface loading.

Extensive studies have shown that the mechanical behavior of lining segments presents obvious nonlinearity (Arnau and Molins 2012). Among these studies, the nonlinear response of lining was usually analyzed by the load structure method where the soil springs were used to simulate the interaction between the tunnel structure and soil when the corresponding structural response was solved under various pre-assumed loading condition. Zhou et al. (2019) proposed a multi-scale simulation method which considered three levels of material, segment and tunnel, and the nonlinear response of the tunnel segment under different ovalisation conditions was analyzed. Based on ADINA software, Chen and Mo (2009) established a refined shield tunnel segment model to elaborately consider bolts and hand holes, and the nonlinear response of the structure under shield thrust and torsion loading were studied. Wang and Zhang (2013) simulated the segments and bolts of the tunnel with solid elements, and the deformation mechanism of the shield tunnel under overloading was analyzed. Based on the numerical analysis of load structure method, a quick insight into the structural damage response can be obtained. However, the simplified soil spring and pre-assumed loading cannot reflect the real lining-ground interaction. Consequently, the authenticity of the simulation results is in doubt.

Another calculation strategy—layer structure method is more preferable to be adopted to involve complex geotechnical conditions such as more realistic lining interaction. In this method, the lining structure, the surrounding stratum and its contact surface are all modeled in detail at the same time. However, to yield a solution, it is necessary to limit the scale of model and the precision meshwork of the FEM model. Papanikolaou and Kappos (2014) studied the structural response and cracking behavior of a horseshoe-shaped tunnel based on ATENA software under various conditions such as fire, blast and earthquake with a plane strain model. Xu et al. (2019) put forward a new numerical approach for cracked segment to analyze the mechanical behavior of lining with multi-cracks, and the cracking mechanism of segmental linings investigated from on-site inspection was revealed by the numerical results.

In addition, some researchers (Sun et al. 2017; Yang et al. 2016) combined the above two mentioned calculation strategies in their studies. Firstly, layer structure method with a homogeneous ring having degraded bending stiffness was adopted to calculate the soil pressure acting on the lining or tunnel ovalisation deformation. Then, the above calculated results were treated as input parameters in the subsequent step which was carried out in the framework of load structure method. In this way, soil pressure acting on the lining and nonlinear response of lining structure are calculated successively and separately. But there are still shortages such as computational complexity and nonobjective simulation on the coupling effect of surrounding soil and linings.

The motivation of the present study is to propose an optimized finite element modelling method in the framework of layer structure method to involve the nonlinear behavior of both the surrounding soil and segments with advanced material models. A two-dimensional model of a real tunnel section of Hangzhou Metro Line 1 is established, where hardening soil model with small strain (HS-small model) and total strain crack

model for reinforced concrete are adopted. A parameter study is performed in order to reveal the influence of the rotation angle of the tunnel, surface loading width, the offset of surface loading and the depth of the tunnel. Based on it, the crack characteristics of tunnel segments under different loading condition are discussed, which can provide an instructive scientific support for the protection and maintenance of existing shield tunnels.

2 Modeling Strategies

To achieve a comprehensively modelling, commercial software DIANA 10.3 was used in the present study. It takes in plenty of advanced material models, while providing a feasible and sufficient numerical tool and making it possible to model the lining and surrounding soil as well as their interaction in detail.

The case is from Hangzhou Metro Line 1 (Xie et al. 2020). The tunnel lining is made with C50 reinforce concrete, and the internal and external diameters of the ring are equal to 5.5 m and 6.2 m respectively. Thus, the lining thickness is equal to 350 mm. The whole ring is divided into 1 key segment (F), 2 adjacent segments (L1, L2) and 3 standard segments (B1, B2, B3). And every ring has a width of 1.2 m, with a rotation angle of 45°between adjacent rings, as shown in Fig. 1. Taking the requirement of convergence for nonlinear analysis into account, the modeling is carried out in two-dimensional and the strengthening effect of the circumferential joint is ignored, which is a more unfavorable case.

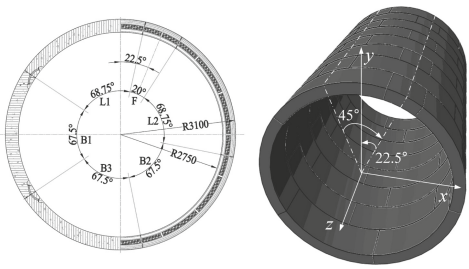

Fig. 1. Configuration of Hangzhou Metro Line 1

2.1 Concrete Behavior

Refer to the local crack direction, the total strain crack model can be divided into rotating, fixed and mixed crack modes. The rotating crack model is adopted in present paper for it was proved to have a better simulation result for reinforced concrete structures (Hendriks et al. 2017). The parameters of segment concrete are shown in Table 1. The exponential model is adopted to describe the tensile softening behavior of concrete, the stress-strain

curve is shown in Fig. 2(a), in which h_{cr} is band width which can be calculated from the element size. G_f^{I} is suggested to derive from the equation (Hendriks et al. 2017):

$$G_f^I = 73 \times f_{cm}^{0.18} \tag{1}$$

Where f_{cm} is mean compression strength, herein f_{cm} equals to 58 MPa.

Table 1. Parameters of C50 concrete

Property	Value
Young's modulus, E(MPa)	34300
Poisson's ratio,v	0.2
Tensile strength, f_t(MPa)	2.64
Compression strength, f_c(MPa)	32.4
Tensile fracture energy, G_f^{I}(N/m)	151
Compression fracture energy, G_c(N/m)	37750

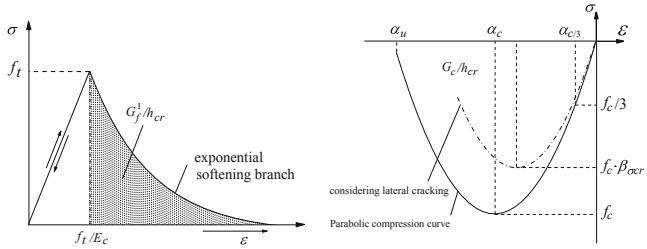

Fig. 2. Stress-strain diagram in tension and compression

The concrete compression curve is shown in Fig. 2(b), and the equation of the parabolic compression curve is defined as follows (Feenstra 1993):

$$\alpha_{c/3} = -\frac{1}{3}\frac{f_c}{E} \tag{2}$$

$$\alpha_c = -\frac{5}{3}\frac{f_c}{E} = 5\alpha_{c/3} \tag{3}$$

$$\alpha_u = \min\left(\alpha_c - \frac{3}{2}\frac{G_c}{hf_c}, 2.5\alpha_c\right) \tag{4}$$

In which α_u is ultimate compressive strain of concrete; α_c is strain at f_c; $\alpha_{c/3}$ is strain at $f_c/3$, when the concrete is in the elastic state.

Considering the fact that the tensile strain in the larger principal strain direction will cause a reduction in the compressive strength of the element perpendicular to it, which is

called the compression softening effect, a reduction factor $\beta_{\sigma cr}$ is adopted to describe the behavior of lateral cracking. $\beta_{\sigma cr}$ is defined by Vecchio and Collins (1993) as follows:

$$\beta_{\sigma cr} = \frac{1}{1 + K_c} \leq 1 \tag{5}$$

$$K_c = 0.27\left(\frac{\varepsilon_1}{\alpha_c} - 0.37\right) \tag{6}$$

2.2 Reinforcement Element

The reinforcement is simplified by the grid element, which can be well embedded in the solid element. The grid element does not participate in mesh division and does not have degrees of freedom as well. It only contributes stiffness by combining with the concrete element. In 2D numerical model, it is performed as a curve. The grid element requires that the actual complex reinforcement is simplified with an equivalent thickness d_{eq}. A local axis *xyz* is applied to the grid element, where the equivalent thickness in *x* axis and *y* axis are derived from longitudinal reinforcement and cross reinforcement respectively. Schematic diagram is as shown in Fig. 3, Where ϕ is the diameter of reinforcement in this local direction, *S* is the corresponding spacing of the reinforcement.

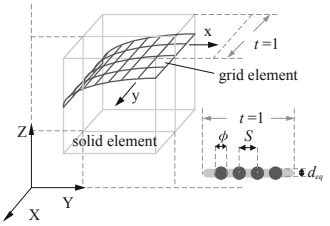

Fig. 3. Schematic diagram of grid reinforcement

Based on design drawing of the shield segment, the reinforcement is simplified into two layers of grid element inside and outside along the thickness direction. Von-Mises plastic strain model is endued to the reinforcement. The parameters of the reinforcement are shown in Table 2.

2.3 Soil Model

HS-small model (Benz 2007) is widely accepted in the numerical simulation of soil such as sand, silt and clay, having access to simulate the nonlinear behavior of soil loading and unloading. The Hyperbolic reduction curve of shear moludus is shown in Fig. 4, where the governing equation of tangent shear modulus is defined as a polyline:

$$G = \begin{cases} G_0\left(\dfrac{\gamma_{0.7}}{\gamma_{0.7} + \alpha\gamma_{Hist}}\right)^2 & \text{for } \gamma_s \leq \gamma_c \\ \dfrac{E_{ur}}{2(1 + v_{ur})} & \text{for } \gamma_s \geq \gamma_c \end{cases} \tag{7}$$

Table 2. Parameters of reinforcement

Property	Value
Young's modulus, E(MPa)	2×10^5
Poisson's ratio,v	0.3
Concrete cover thickness, c(mm)	60
Equivalent thickness, f_c(mm)	1.979 (outside)
	2.037 (inside)
Yielding strength, f_y(MPa)	335
Ultimate strength, f_u(MPa)	455

$$\gamma_c = \frac{\gamma_{0.7}}{0.385}\left(\sqrt{\frac{G_0}{G_{ur}}} - 1\right) \tag{8}$$

In which G_0 is small strain shear stiffness; $\gamma_{0.7}$ is the threshold shear strain when $G = 0.7G_0$; γ_c is the cut-off shear strain which is derived from Hardin-Drnevich relationship, as shown in Eq. (8); γ_{Hist} is the history strain; E_{ur} is the unloading-reloading stiffness; v_{ur} is the Poisson's ratio for unloading-reloading, which is equal to Poisson's ratio v by default and is a constant value.

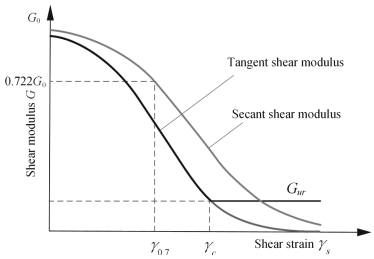

Fig. 4. Hyperbolic curve of shear modulus

The unloading-reloading stiffness E_{ur} and small strain shear stiffness G_0 are subject to depend on the current pressure according to the following power laws:

$$G_0 = G_0^{ref}\left(\frac{p_t' + p'}{p_{ref}'}\right)^m \tag{9}$$

$$E_{ur} = E_{ur}^{ref}\left(\frac{p_t' + p'}{p_{ref}'}\right)^m \tag{10}$$

In which G_0^{ref} is the reference small strain shear stiffness; E_{ur}^{ref} is the unloading-reloading shear stiffness; p_{ref}' is the reference pressure for stiffness; m is the power for stress-level

dependency of stiffness (default $m = 0.5$); p_t' is a tensile pressure to ensure non-zero stiffness.

In order to facilitate the parameter analysis, the typical soil layer ③$_5$ in the real case is selected as a single layer. The parameters of the soil layer in HS-small model are shown in Table 3.

Table 3. Parameters of soil with HS-small model

Property	Value
Natural unit weight, ρ(kg/m^3)	1860
Poisson's ratio,v	0.2
Friction angle, ϕ(°)	6.5
cohesion, c(kPa)	29
Threshold shear strain, $\gamma_{0.7}(10^{-4})$	2
Reference pressure, p'_{ref}(kPa)	100
Reference small strain shear stiffness, G_0^{ref} (MPa)	43.8
Unloading-reloading shear stiffness, E_{ur}^{ref} (MPa)	24.3

2.4 Interaction Models

The interfaces included in the numerical model are structure-ground interface and longitudinal joint interface between segments. The structure-ground interface is simulated by Coulomb friction contact, and the friction angle of $\sin\varphi = 0.3$ is taken to illustrate the small sliding (Liu 2012).

Longitudinal joint is a three-dimensional complex contact where plenty materials need considering. Its contact behavior is closely related to packer, concrete and bolts. Thus, the simplified of longitudinal joint is essential in the layer-structure model. Herein the longitudinal joint is simplified as a two-dimensional 6-node line interface. It has been proved by comparison with full-scale test results that this simplified method can effectively illustrate the nonlinear behavior of longitudinal joint (Yang et al. 2016). The stiffness of interfaces is as shown in Table 4.

2.5 Mesh Strategies and Construction Phase

According to the covering soil of the real case, the surface loading is simplified to a trapezoidal load. CQ16E eight-node quadrilateral element is adopted in the mesh work, and different mesh sizes are set for soil and tunnel structure respectively. The size of the soil element is 1m, while the lining element is 0.05 m. Thus, the segment in thickness id divided into 6 elements which meets the requirements of nonlinear analysis for concrete structures. The mesh work of the model is shown in Fig. 5. The construction phase is performed with four steps. First step is the initial phase which balances the ground

Table 4. Interface stiffness

Property	Ground-structure	Longitudinal joint
Type	Coulomb friction	Linear elastic
Normal stiffness, k_n(N/m^3)	2×10^{12}	1×10^{12}
Shear stiffness, k_s(N/m^3)	1×10^{8}	3×10^{10}
Friction angle, $\varphi(^\circ)$	17.45	-

stress. Then the linings and its interface are activated. In the third phase the soil in the tunnel is freezed to simulate tunnel excavation. After the tunnel excavation, the previous displacement is cleared, and the surface load is activated when the load factor is set to 0, 0.25, 0.5, 0.75 and 1.0 in turn.

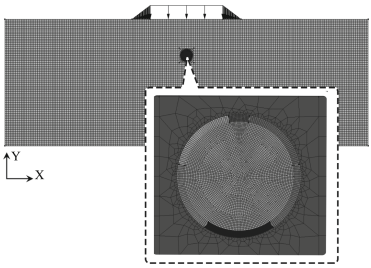

Fig. 5. FEM model and meshing

3 Parameter Analysis

Herein a sensitivity analysis is performed with several parameters of interest such as the rotation angle of the ring, loading width, the offset of loading and the depth of the tunnel. The schematic model is shown in Fig. 6, where x_1 and x_2 are the upper top width and the isosceles width of the trapezoid load respectively; q_0 represents the value of uniform load. Herein x_2 and q_0 are set to fixed value, which equal to 10 m and 140 kPa. Hence, the loading range can be defined by x_1. To analyze the influence of different assembly location for segments, an angle denoted by θ was used to define the relative rotation of the assembling lining. For example, when $\theta = 0$, the key segment is located at vault. Meanwhile, d and h denote the offset of loading and the depth of the tunnel. The parameters of cases are shown in Table 5.

In order to evaluate the damage state of the lining comprehensively, indicators of crack ratio (Yang et al. 2016) and crack index I_{cr} are introduced. They are used to evaluate the overall damage of the lining and predict the development of the cracks respectively, which are defined as:

$$\text{crack ratio} = \frac{\text{quantity of cracking integration points}}{\text{quantity of integration points of linings in total}} \times 100\% \tag{11}$$

Table 5. Case studies

Case	θ(°)	d(m)	x_1(m)	h(m)
1	0	0	40	15
2	22.5	0	40	15
3	45	0	40	15
4	22.5	10	40	15
5	22.5	20	40	15
6	22.5	30	40	15
7	22.5	0	200	15
8	22.5	0	20	15
9	22.5	0	10	15
10	22.5	0	40	25
11	22.5	0	40	35
12	22.5	0	40	45

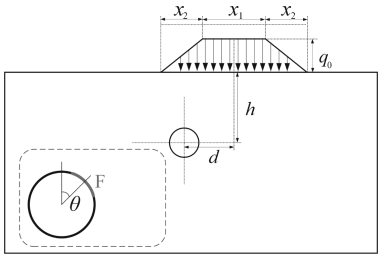

Fig. 6. Schematic model

$$I_{cr} = \frac{f_t}{\sigma_1} \tag{12}$$

4 Analysis of Results

Figure 7 and 8 show the result of lining response of the cases given in the Table 4. The outer rings in Fig. 7 illustrate the contours of crack width, while the colored area of the contour indicates that the current area has reached the damage state. Meanwhile, it can be summed up that all the calculation cases show similar 4 crack area, which are the inner side of the vault and arch bottom, as well as outer side of the left and right hance. The inner rings in Fig. 7 illustrate the contours of I_{cr} with an absolute deformation of 50 times. According to the definition of Eq. (9), I_{cr} can be regarded as a safety margin of concrete. The closer its value is to 1, the more likely it cracks. Hence, the red area in contours is treated as "safe zone" where the tensile strength is much larger than the

current principal stress, and the blue area is the "danger zone" that cracks have occurred or are about to appear. The influence of several parameters is set forth in subsequent sections respectively.

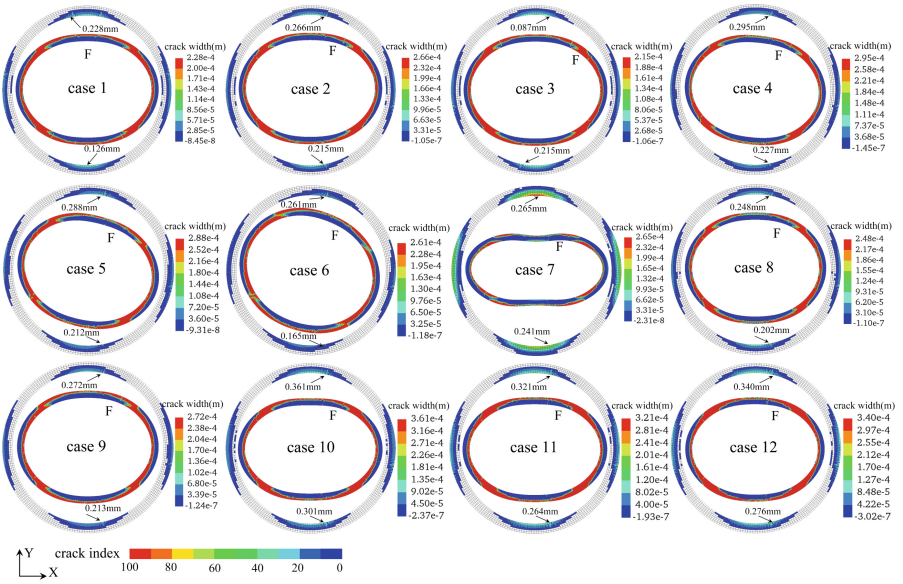

Fig. 7. Crack width and crack index contour (deformation enlarged 50 times) when load factor = 1

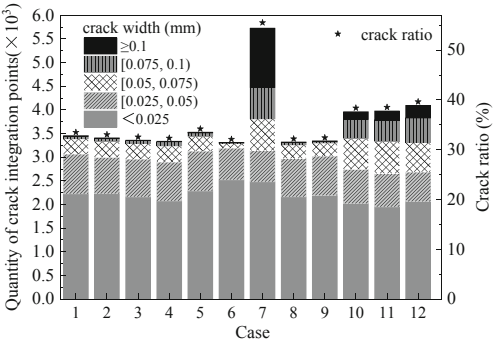

Fig. 8. Quantities of crack integration points when load factor = 1

4.1 Influence of Rotation Angle of the Ring

As aforementioned, the angle θ represents the overall rotation of the longitudinal joint position, thus it affects the force mechanism under loading of the tunnel at the same time. θ in cases 1–3 is set to 0°, 22.5° and 45° respectively.

It can be seen from Fig. 7 that when θ changes, the ovalisation and cracking area of the linings are basically unaltered, but the maximum crack width and its occurrence position changes due to the rotation of the longitudinal joint position. The occurrence position of maximum crack width often appears on one side of the longitudinal joint. However, it does not appear in the F segment, for the F segment is much shorter which leads to further stress release. When θ is 0°, the cracking contour is symmetrical; when it is 22.5°, the maximum crack width on the inner side of the vault and arch bottom increases; when it is 45°, there is no longitudinal joint in the cracked area inside the vault. Consequently, the maximum crack width of the vault decreases to 0.087 mm.

The I_{cr} contour shows that as θ increases, the distribution of the "danger zone" is basically unaltered, only slightly distinguished at each joint position. It can be seen from Fig. 8 that as θ increases, the cracking rate slightly decreases. When Load factor = 1, the cracking rates of three cases are 33.5%, 33.0%, and 32.5% respectively. To sum up, the increase of θ affect the internal force distribution of the ring due to joint shifting, and slightly improve the ability of crack resisting of the ring.

4.2 Influence of the Load Offsetting

Load offsetting is an important factor for the delimiting of the subway protection area, herein the influence of the load offsetting on the tunnel response is studied in cases 4–6. Figure 7 shows that when d increases, the four main crack areas rotate clockwise, while the I_{cr} contours also turn out with similar changes. When $d = 10$ m, the crack width on the vault and the arch bottom reaches maximum. As d increases, the maximum crack width decreases on the contrary.

Figure 9 show the change rule of newly added crack integration points when d increases from 0 to 100 m. When $d = 20$ m, the crack ratio reaches the maximum which equals to 34.2% when load factor = 1. when d is greater than 30 m, the crack ratio keeps dropping. During the offset of the surface loading, the horizontal displacement field where the tunnel is located changes, which means a forcible displacement in the opposite direction of d is imposed on the tunnel. Therefore, even if the load is not exactly symmetric with the tunnel, the tunnel may still have an even more unfavorable development trend of crack disease.

When the load factor = 0.25, incremental crack integration points decrease significantly when d increases. When d is greater than 50 m, the surface loading can barely cause an adverse effect of the lining. But in the subsequent load steps, the incremental crack integration points grow obviously when d approaches 100 m. Hence, the effect of load offsetting on the lining response still links to the magnitude of the surface loading. To sum up, the load offsetting will cause the overall rotation of the tunnel structure and crack area. Within a certain offsetting range, it may bring more adverse effects such as the increase of the maximum crack width and crack ratio. But when d is greater than 30 m in the case, the crack ratio keeps dropping as d increases.

4.3 Influence of Load Width and Buried Depth of Tunnel

The parameter analysis of cases 7–9 and cases 10–12 are carried out for x_1 and h respectively. Case 7 sets x_1 to 200 m, its crack ratio reaches to 55%, which is much higher than

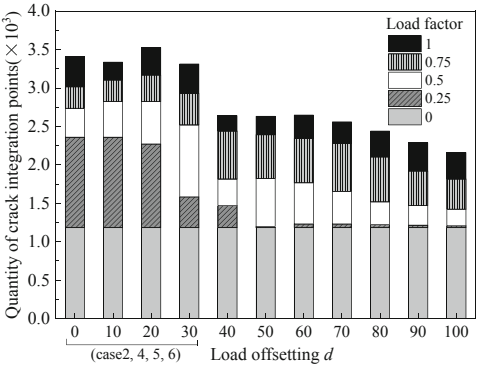

Fig. 9. Quantities of incremental crack integration points in each load case

any other cases, and the crack area has been extended to the full ring. Case 8 and Case 9 reduce x_1 to 20 m and 10 m, whose crack ratios are 32.2% and 32.4% respectively.

h in cases 10–12 are 25 m, 35 m and 45 m respectively, whose crack ratio are 38.4%, 38.5% and 39.6%. The reason why it leads to a slight increase on the crack ratio as h increases can be explained as follows. Herein, the surrounding soil is treated as soft soil, while the stress redistribution after the tunnel excavation is considered. Therefore, as buried depth increases, the stress condition of the tunnel deteriorates before surface loading. As a result, the increase in buried depth under surface loading in soft soil area may not bring beneficial effects.

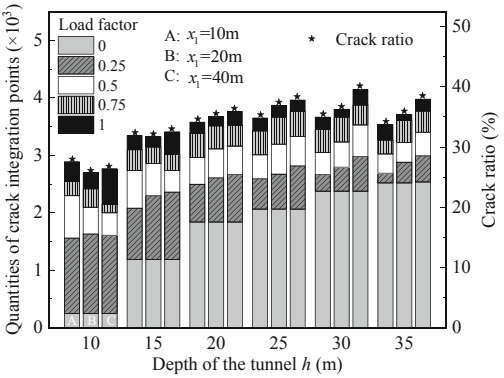

Fig. 10. Effect on crack state of load width and tunnel depth

Considering that the width of the surface loading effects the depth of the additional stress field, it is inappropriate to separate load width from the buried depth of the tunnel in the parameter analysis. Therefore, supplementary cases of double-factor parameter analysis are carried out, as illustrated in Fig. 10. When h is less than 15 m, the crack ratio under the 10 m-width surface loading is the highest, followed by 40 m and 20 m;

when h is equal to 15 m, the crack ratio of three load widths is basically the same; when h continues to increase, the larger the loading width is, the higher the crack ratio will be.

From the perspective of the effect of buried depth on crack ratio, as h increases, the effect of the surface load on the crack ratio decreases. However, if the adverse effect of stress redistribution after the tunnel excavation is considered, as h increases, the crack ratio will increase first and then decrease, while the peak of crack ratio is regarded as the most unfavorable buried depth. $x_1 = 10$ m corresponds to the most unfavorable burial depth about 25 m, with a crack ratio of 35.3%; $x_1 = 20$ m corresponds to the most unfavorable burial depth about 25 m, with a crack ratio of 37.4%; $x_1 = 40$ m corresponds to the most unfavorable burial depth about 30 m, with a crack ratio of 40.2%.

4.4 Discussion on the Relationship Between Ovalisation and Crack Ratio

Several parameters discussed above can affect the tunnel crack state to varying degrees. However, they cannot be separated to establish a direct relationship with current crack state. The crack rate is an evaluation index for lining damage state which is difficult to obtained by detection in reality, hence it is vital to establish a connection between the crack ratio and commonly used monitoring index.

Tunnel ovalisation, as a commonly used structural evaluation index, has been proved to evaluate the tunnel structural performance effectively (Shao et al. 2016; Wang and Zhang 2013; Zhou et al. 2019). Based on the calculation results in Sect. 4.3, the fitting curve of the relationship between the horizontal ovalisation and crack ratio is carried out, as shown in Fig. 11. The results show that the power function curve fits well with the scatter plot, revealing the nonlinear relationship between crack ratio and the horizontal ovalisation: as horizontal ovalisation increases, the crack ratio increases but the its growth rate slows down. Therefore, the power function can be used as a simple method to evaluate the damage state of tunnel ring.

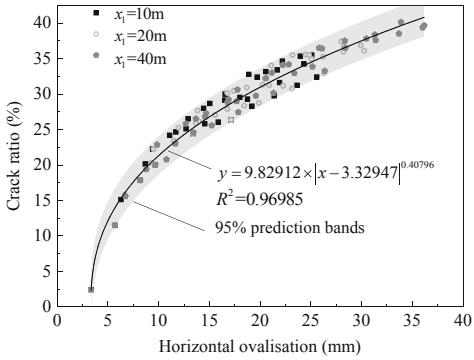

Fig. 11. Relationship curve of horizontal ovalisation and crack ratio

5 Conclusions

Based on the layer structure method, a two-dimensional numerical modelling for segmental lining subjected to surface loading involving the nonlinear behavior of both soil

and lining is carried out. Thereby a direct connection between surface loading, soil and tunnel is performed, which realizes a one-step numerical simulation from surface loading to structural response. The following conclusions can be drawn through the parameter study:

- Maximum crack width, crack index, and crack ratio are introduced to evaluate the damage characteristics of linings. Maximum crack width points out the most detrimental area where diseases are most likely to occur in practice. The crack index evaluates the tensile safety margin of structure, thereby predicting the trend of further cracking. The crack ratio clarifies the percentage of cracked integration points, which can be regarded as an important indicator to evaluate the overall damage state of the ring.
- The increase of rotation angle of the ring affects the internal force distribution of the ring, and slightly improves the crack-resistant ability of the ring. Within a certain offset range, the offset of the non-axisymmetric surface loading may bring consequences like the overall rotation of the damage zone, growth in the crack ratio and increasing in the maximum crack width. But when d is greater than 30 m in the case, the crack ratio keeps dropping as d increases.
- Double-factor parameter analysis for the width of the surface loading and the buried depth of the tunnel shows that when the tunnel is buried shallow, a surface loading whose width is too small or too large will lead to an increase in crack ratio. When it is buried deeper, a larger load width has a greater impact on crack response. If the stress redistribution after tunnel excavation is not taken into consideration, the increase in buried depth can effectively reduce the adverse effects of surface loads. However, if the adverse effects of surface load and stress redistribution after excavation are considered at the same time, there is an unfavorable buried depth that maximizes the crack ratio of the tunnel.
- The fitting curve of the relationship between the crack ratio and the horizontal ovalisation performs a power function: as horizontal ovalisation increases, crack ratio increases rapidly at the beginning, while the growth rate continues to slow down. However, the function's applicability in other types of shield tunnel needs verifying. Still, it has a wide range of applications for the standard ring in the case is universal in metro tunnels and road tunnels. Consequently, this power function can be used as a simple method to evaluate the damage state of the tunnel ring.
- Carried out in a two-dimensional model, the study only focuses on the transverse ovalisation of the tunnel ring and its longitudinal crack characteristics, when the impact of the three-dimensional assembly effect is ignored. The longitudinal deformation of the tunnel has a more complicated impact on the crack behaviors both in the longitudinal and circumferential directions, which needs figuring out in the future work.

References

Shao, H., Huang, H.W., Zhang, D.M., Wang, R.L.: Case study on repair work for excessively deformed shield tunnel under accidental surface surcharge in soft clay. J. Chin. J. Geotech. Eng. **38**(6), 1036–1043 (2016)

Arnau, O., Molins, C.: Three dimensional structural response of segmental tunnel linings. J. Eng. Struct.. **44**, 210–221 (2012)

Zhou, B., Xie, X.Y., Yang, Y.B., Wang, X.J.: Service performance evaluation and cross scale simulation of shield tunnel during overhaul. J. Tongji Univ. (Nat. Sci.) **47**(10), 1390–1397 (2019)

Chen, J.S., Mo, H.H.: Numerical study on crack problems in segments of shield tunnel using finite element method. J. Tunnel. Undergr. Space Technol. **24**(1), 91–102 (2009)

Wang, R.L., Zhang, D.M.: Mechanism of transverse deformation and assessment index for shield tunnels in soft clay under surface surcharge. J. Chin. J. Geotech. Eng. **35**(6), 1092–1101 (2013)

Papanikolaou, V.K., Kappos, A.J.: Practical nonlinear analysis of unreinforced concrete tunnel linings. J. Tunnel. Undergr. Space Technol. **40**, 127–140 (2014)

Xu, G., He, C., Lu, D., Wang, S.: The influence of longitudinal crack on mechanical behavior of shield tunnel lining in soft-hard composite strata. J. Thin. Walled Struct. **144**, 106282 (2019)

Sun, L.W., Qin, J.S., Hong, Y., Wang, L.Z., Zhao, C.J., Qin, X.: Shield tunnel segment and circumferential joint performance under surface surcharge. J. ZheJiang Univ. Eng. Sci. **51**(8), 1509–1518 (2017)

Yang, Y.B., Zhou, B., Xie, X.Y.: Study on transverse deformation and cracking property of shield-driven tunnel induced by adjacent excavation. J. Chin. J. Rock Mech. Eng. **35**, 4082–4093 (2016)

Xie, J.C., Wang, J.C., Huang, W.M.: Nonlinear structural analysis on cracking behavior of TBM tunnel segment under surface loading. J. Railway Sci. Eng. in press (2020)

Hendriks, M.A.N., de Boer, A., Belletti, B.: Guidelines for nonlinear finite element analysis of concrete structures. J. Rijkswaterstaat Technisch Document (RTD), Rijkswaterstaat Centre for Infrastructure, RTD **1016** (2017)

Feenstra, P.H.: Computational aspects of biaxial stress in plain and reinforced concrete. PhD thesis, Delft University of Technology, Delft, The Netherlands (1993)

Benz, T.: Small-strain stiffness of soils and its numerical consequences. PhD thesis, University of Stuttgart, Institute of Geotechnik, Stuttgart, Germany (2007)

Vecchio, F.J., Collins, M.P.: Compression response of cracked reinforced concrete. J. Struct. Eng. **119**(12), 3590–3610 (1993)

Liu, H.: Three-dimensional analysis of underground tunnels in liquefiable soil subject to earthquake loading. In: GeoCongress 2012: State of the Art and Practice in Geotechnical Engineering, pp. 1819–1828 (2012)